
**Separation Science and Technology**
Publication details, including instructions for authors and subscription information:
http://www.informaworld.com/smpp/title~content=t713708471

# Groundwater Cleanup by In-Situ Sparging. XIV. An Air Channeling Model for Biosparging with a Horizontal Pipe

David J. Wilson; Robert D. Norris; Ann N. Clarke

**To cite this Article** Wilson, David J. , Norris, Robert D. and Clarke, Ann N.(1998) 'Groundwater Cleanup by In-Situ Sparging. XIV. An Air Channeling Model for Biosparging with a Horizontal Pipe', Separation Science and Technology, 33: 1, 97 — 118
**To link to this Article: DOI:** 10.1080/01496399808544758
**URL:** http://dx.doi.org/10.1080/01496399808544758

SEPARATION SCIENCE AND TECHNOLOGY, 33(1), pp. 97–118, 1998

# Groundwater Cleanup by In-Situ Sparging. XIV. An Air Channeling Model for Biosparging with a Horizontal Pipe

DAVID J. WILSON, ROBERT D. NORRIS, and ANN N. CLARKE
ECKENFELDER INC.
227 FRENCH LANDING DRIVE, NASHVILLE, TENNESSEE 37228, USA



## ABSTRACT

A mathematical model is developed for biosparging with a horizontal slotted pipe. Biological processes are handled by means of Monod kinetics; biomass, oxygen, and substrate concentrations are assumed to be significant. The injected air is assumed to move through persistent channels in the aquifer. Distributed nonaqueous phase liquid may be present. The dependence of model results on some of the model parameters is explored. The sparging and biosparging of nonaqueous phase liquid volatile organic compounds of quite low water solubility (such as *n*-octane) are shown to be extremely slow. High dispersivities (perhaps the result of pulsed air injection) result in very markedly increased remediation rates.

## INTRODUCTION

The use of air sparging and biosparging for the cleanup of aquifers contaminated with volatile and/or biodegradable organic compounds is becoming more common, and it has been discussed in several recent books and reports (1–6, for example).

It is now known that when air is injected into an aquifer it moves up to the water table in persistent channels, rather than as random, isolated bubbles, and that the steady injection of air into an aquifer does not generate a bulk circulation of water in the vicinity of the injection well (2, 7–11). The implications of these facts for the rate of mass transport of volatile

organic compounds (VOC) from the aquifer to the sparging gas are unpleasant, and suggest that initial optimism about the technique was excessive. Nevertheless, a recent review of sparging case studies by Bass and Brown (12) indicates that, in fact, sparging generally performs rather well. Sparging models which we have developed and which include air channeling show reasonably rapid rates of remediation (13–15). A somewhat more sophisticated approach used by Clayton (16), which includes both pore and macroscopic scale air fingering, also yielded reasonably fast remediations.

We recently published a mathematical air channeling model for biosparging in a one-dimensional laboratory column (17). Monod kinetics were used to describe the biological processes, and it was assumed that oxygen, biomass, and substrate provided an adequate description of these—that nitrate, phosphate, etc. were not growth-limiting and their concentrations could therefore be ignored.



The model omits consideration of the sorption of contaminant on the aquifer medium. Sorption, if it occurs to any significant extent, will increase the time required for cleanup in two ways. First, the sorption equilibrium decreases the concentration of contaminant dissolved in the aqueous phase, thereby also reducing the gas-phase concentration via Henry's law. Second, the kinetics of desorption may be quite slow. Fortunately, sorption is not generally a serious problem with common organics of low molecular weight.

Here we apply the above approach to biosparging to sparging with a horizontal slotted pipe, a configuration currently in use at Savannah River. The mathematical complexity of the system is such that a full-fledged two- or three-dimensional biosparging model for microcomputers strains the resources presently available. Therefore the approach used is to first mathematically construct "tubes of influence" around air channels, and then to examine the biosparging of contaminant in selected tubes of influence.

The next section of the paper presents the physical picture of biosparging being examined and the mathematical analysis. This is followed by a section on results.

## ANALYSIS

The system geometry addressed here is that of a long horizontal sparging pipe as indicated in Fig. 1. Cartesian coordinates $x$ (horizontal) and $z$ (vertical) are used, and the $z$-component of the molar gas flux field is postulated in the same way as was done in an earlier sparging model (18). The air is then assumed to move in persistent channels, the density of

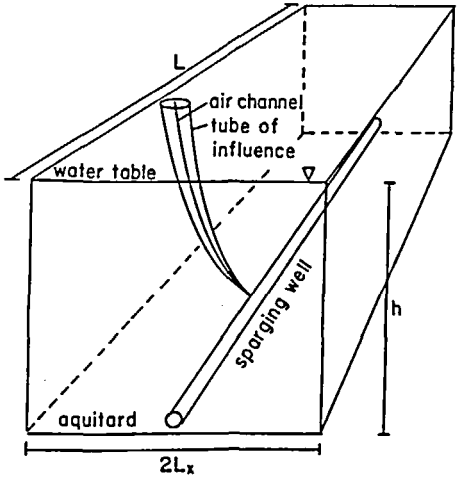


FIG. 1 Schematic diagram of the geometry of the horizontal biosparging well being modeled.



which in any particular region is proportional to the local volumetric gas flux. The solution of nonaqueous phase liquid (NAPL) droplets, if present, is also handled as it was in that paper; the rate of solution of a NAPL droplet is assumed to be controlled by the rate of steady-state diffusion of VOC through a stagnant aqueous boundary layer around it. Dissolved VOC moves through the aqueous medium to the air channels by dispersion, and oxygen moves from the air channels into the aqueous medium by the same mechanism. Oxygen and VOC boundary conditions at the air channel–water interface are assumed to be governed by Henry's law.

Biodegradation of VOC is handled by Monod kinetics, and a factor permitting toxic inhibition by excessively high concentrations of VOC is included. This approach was used in the earlier model for biosparging in a column (17). Modeling of biodegradation requires the inclusion of biomass and dissolved oxygen in addition to the NAPL and dissolved VOC required for the modeling of simple air sparging. Modeling of biodegradation also adds substantially to the quantity of computation which must be carried out for each time step in the numerical integration. These factors make the development of a full-fledged two-dimensional model for presently available personal computers infeasible; the time and RAM requirements of such a model would be too great.

We therefore turn to the task of modeling the biosparging process in the tube of influence around a single air channel, which is assumed to

follow along a streamline of the volumetric gas flux field. A tube of influence is that portion of the aquifer from which VOC diffuses to the air channel running along its axis. One of these tubes of influence is indicated in Fig. 1, and a schematic drawing of a tube "straightened out" and partitioned for mathematical analysis is shown in Fig. 2. The partitioning of one of the tube segments $\Delta V_i$ into annular volume subelements $\Delta V_{ij}$ is shown in Fig. 3. Dispersion transport takes place between the annular volume subelements, and between the innermost one of them and the air channel.

The analysis is as follows. Let

$L$ = length of horizontal slotted sparging pipe, m
$h$ = depth of sparging pipe below the water table, m
$L_x$ = half-width of the domain of interest, m
$q$ = volumetric air flow rate, standard $m^3/s$
$Q$ = molar air flow rate, mol/s
$a$ = lateral half-range of air flow at top of aquifer, m
$m$, $n$ = exponents describing the gas flow pattern. See Eq. (1)
$v_x'$ = $x$-component of the molar air flux, $mol/m^2 \cdot s$
$v_z'$ = $z$-component of the molar air flux, $mol/m^2 \cdot s$
$v_x$ = $x$-component of the superficial air flow velocity, $m^3/m^2 \cdot s$
$v_z$ = $z$-component of the superficial air flow velocity, $m^3/m^2 \cdot s$
$s$ = arc length measured from the air injection pipe along an air flow line, m
$n_s$ = number of cylindrical volume elements $\Delta V_i$ into which the tube of influence about an air channel is partitioned for analysis



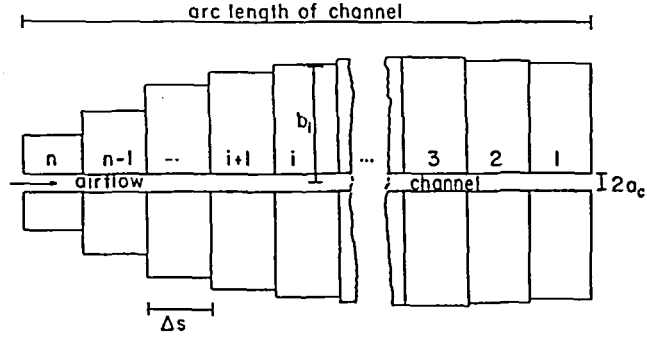


FIG. 2 Mathematical partitioning of the tube of influence surrounding an air channel.

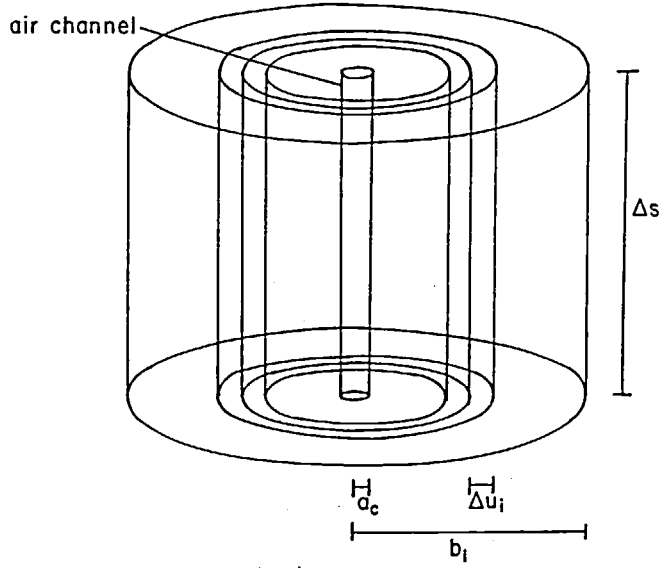


FIG. 3 A single section of a tube of influence showing the annular volume elements used in the modeling of dispersion.



$n_u$ = number of annular volume subelements $\Delta V_{ij}$ into which the volume element $\Delta V_i$ is partitioned for modeling dispersion
$b_i$ = radius of $\Delta V_i$, m
$\Delta u_i$ = thickness of the annular wall of $\Delta V_{ij}$, m
$P(z)$ = hydrostatic pressure at height $z$ above the air injection pipe, atm
$\sigma$ = 0.09675 atm/m
$a_c$ = mean radius of air channel, m
$x_{max}$ = $x$-coordinate of the center of the upper end of the tube of influence of interest, m
$v$ = porosity of aquifer medium, dimensionless
$\rho_{soil}$ = density of saturated aquifer medium, kg/m$^3$
$D_s$ = dispersivity of VOC and dissolved $O_2$, m$^2$/s
$D_f$ = diffusivity of VOC, m$^2$/s
$\rho_{VOC}$ = density of NAPL VOC, kg/m$^3$
$K_H$ = Henry's constant of VOC, dimensionless
$C_{sat}$ = aqueous solubility of VOC, kg/m$^3$
$a_d$ = mean NAPL droplet radius, m
$C_0^N$ = initial NAPL concentration, kg/m$^3$ of soil
$C_0^W$ = initial dissolved VOC concentration, kg/m$^3$ of water

$C_{ij}^{N}$ = NAPL concentration in $\Delta V_{ij}$, kg/m$^3$ of soil
$C_{ij}^{W}$ = dissolved VOC concentration in $\Delta V_{ij}$, kg/m$^3$ of water
$C_i^g$ = channel gas phase VOC concentration in $\Delta V_i$, kg/m$^3$
$O_0^g$ = gas phase $O_2$ concentration in injected gas, kg/m$^3$
$O_i^g$ = channel gas phase $O_2$ concentration in $\Delta V_i$, kg/m$^3$
$O_{ij}^{W}$ = dissolved $O_2$ concentration in $\Delta V_{ij}$, kg/m$^3$
$K_O$ = Henry's constant of $O_2$, dimensionless
$K_{bio}$ = Monod specific rate factor for biodegradation, kg/m$^3$·s
$k_{die}$ = first order biomass die-off constant, s$^{-1}$
$B_{ij}$ = biomass concentration, kg/m$^3$ of soil
$B_{1/2}$ = biomass Monod parameter, kg/m$^3$ of soil
$C_{1/2}^{W}$ = VOC Monod parameter, kg/m$^3$ of water
$O_{1/2}^{W}$ = dissolved $O_2$ Monod parameter, kg/m$^3$ of water
$C_{tox}^{W}$ = VOC toxic inhibition parameter, kg/m$^3$ of water
$n_{tox}$ = VOC toxic inhibition exponent, dimensionless
$n_{bio}$ = weight biomass formed/weight VOC consumed
$n_{oxy}$ = weight oxygen consumed/weight VOC consumed
$\Delta t$ = time increment in numerical integration, s

## Gas Flow

We avoid a difficult problem in multiphasic flow by postulating a physically reasonable form for the $z$-component of the molar gas flux. The right half of the domain of interest is modeled. Postulate

$$\begin{aligned} v_z'(x, z) &= A(z)\cdot[(z/h)^m - (x/a)^n], \qquad x < a(z/h)^{m/n} \\ &= 0, \qquad x > a(z/h)^{m/n} \end{aligned} \tag{1}$$

The function $A(z)$ is obtained from the requirement that

$$Q = 2LA(z)\int_0^{a(z/h)^{n/m}} [(z/h)^n - (x/a)^n]dx \tag{2}$$

This yields

$$A(z) = \frac{Q(n+1)}{2Lan}(z/h)^{-(m+m/n)} \tag{3}$$

The $x$-component of the molar gas flux, $v_x'$, is obtained from the requirement that

$$\nabla\cdot\mathbf{v}' = 0 \tag{4}$$

or

$$\frac{\partial v_x'}{\partial x} + \frac{\partial v_z'}{\partial z} = 0 \tag{5}$$

where

$$v_z' = \frac{Q(n+1)}{2Lan}(z/h)^{-(m+m/n)}[(z/h)^m - (x/a)^n] \quad (6)$$

Equation (6) is differentiated with respect to $z$, $\partial v_x'/\partial x$ is obtained from Eq. (5), and integrated from 0 to $x$ to give $v_x'$. The result is

$$v_x' = \frac{Q(n+1)mx}{2Lahn^2}(z/h)^{-(1+m+m/n)}[(z/h)^m - (x/a)^n] \quad (7)$$

The mean superficial gas velocity v is then given by

$$\mathrm{v} = \mathrm{v}'RT/P(z) \quad (8)$$

where $R$ is the gas constant ($m^3$·atm/mol·deg), $T$ is the temperature (deg K), and $P(z)$ is the hydrostatic pressure at a height $z$ above the well. $P(z)$ is given by

$$P(z) = \sigma(h - z) + 1 \text{ atm} \quad (9)$$

Streamlines are obtained by integrating the equation

$$\frac{dz}{dx} = \frac{v_z}{v_x} = \frac{nz}{mx} \quad (10)$$

which yields

$$x(z) = x_{\text{top}}(z/h)^{m/n} \quad (11)$$

## Tubes of Influence

Consider an air channel which terminates at $x_{\text{top}}$, as shown in Fig. 1. Its arc length from the pipe to any elevation $z$ is given by

$$s(z) = \int_0^z [1 + (dx/dz)^2]^{1/2} dz \quad (12)$$

where $dx/dz$ is obtained from Eq. (11). The mean superficial velocity of the air at any point $(x, z)$ along the trajectory is given by Eqs. (6), (7), and (8). The mean superficial speed is then given by

$$|v| = (v_x^2 + v_z^2)^{1/2} \quad (13)$$

It is assumed that the air channel density is directly proportional to $|v|$:

$$\text{number of air channels per unit area} = K|v| \quad (14)$$

The cross-sectional area of the tube of influence around a channel at $z$ is therefore given by $1/(K|v|)$, and the radius of the tube of influence at a

height $z$ along the channel is given by

$$b(z) = 1/[\pi K|v(z)|]^{1/2} \tag{15}$$

The arc length $s$ of the streamline along which the channel is assumed to run is calculated, and the tube of influence is partitioned into $n_s$ volume elements $\Delta V_i$, each of length $\Delta s = s/n_s$. These volume elements are approximated as cylinders, each having a radius $b_i$, where

$$b_i = 1/[\pi K|v(z_i)|]^{1/2} \tag{16}$$

and

$$z_i = z[(i - 1/2)\Delta s], \qquad i = 1, 2, \ldots, n_s \tag{17}$$

See Fig. 2.

The gas flow through the air channel is given by

$$q_{\text{channel}} = |v|\pi b^2 = 1/K \tag{18}$$

independent of the channel being considered or the position along the channel.



## Biological Processes

See Fig. 3 for the partitioning of a cylindrical volume element $\Delta V_i$ into a set of annular volume subelements $\Delta V_{ij}$. The rate of change of aqueous VOC concentration in the $ij$th subelement due to biodegradation is represented by

$$\left[\frac{\partial C_{ij}^{W}}{\partial t}\right]_{\text{bio}} = -K_{\text{bio}} \frac{B_{ij}}{B_{1/2} + B_{ij}} \frac{C_{ij}^{W}}{C_{1/2}^{W} + C_{ij}^{W}} \frac{O_{ij}^{W}}{O_{1/2}^{W} + O_{ij}^{W}} \frac{1}{1 + (C_{ij}^{W}/C_{\text{tox}}^{W})^{n\text{tox}}} \tag{19}$$

The first three factors on the right are the usual Monod kinetics factors; the fourth factor permits inclusion of inhibitory effects of excessively high aqueous concentrations of the VOC if desired. No effects of such nutrients as nitrate or phosphate are included, since such effects are usually not observed, the additional parameters would be difficult to assign, and the computational complexity of the model would be increased.

The rate of change of biomass concentration $B_{ij}$ is then assumed to be given by

$$\frac{dB_{ij}}{dt} = -n_{\text{bio}}\left[\frac{\partial C_{ij}^{W}}{\partial t}\right]_{\text{bio}} - k_{\text{die}}B_{ij} \tag{20}$$

where the second term on the right corresponds to biomass die-off. Typically, $n_{bio}$ is approximately 0.5. The biomass is assumed to be attached and stationary.

The rate of change of the dissolved oxygen concentration associated with biological activity is taken to be

$$\left[\frac{\partial O_{ij}^{W}}{\partial t}\right]_{bio} = n_{oxy}\left[\frac{\partial C_{ij}^{W}}{\partial t}\right]_{bio} \tag{21}$$

Since no term is included for the oxygen demand of decomposing biomass, the value of $n_{oxy}$ is assumed to be that appropriate for the total mineralization of the VOC, which can readily be calculated from the stoichiometry of the reaction for the oxidation of the VOC to $CO_2$, water, etc. Values of $n_{oxy}$ are typically in the 3–3.5 range.



## Dispersion Transport of Aqueous VOC and Dissolved Oxygen

The geometry under consideration is shown in Fig. 3. Dissolved VOC moves by dispersion to the central air channel, while oxygen is dissolved at the air channel/water interface and then moves by dispersion away from the air channel. The thickness of the annular wall of $\Delta V_{ij}$ is given by

$$\Delta u_i = (b_i - a_c)/n_u \tag{22}$$

where $a_c$ is the air channel radius and $b_i$ is the radius of $\Delta V_i$, the $i$th volume element along the air channel of interest. The inner radius of this volume subelement is

$$r_{ij} = a_c + (j - 1)\Delta u_i \tag{23}$$

Then

$$\Delta V_{ij} = \pi \Delta s(r_{i,j+1}^2 - r_{ij}^2) \tag{24}$$

Mass balances with respect to dispersion transport lead to

$$\left[\frac{\partial C_{ij}^{W}}{\partial t}\right]_{disp} = \frac{2\pi D_s \Delta s}{\nu \Delta V_{ij} \Delta u_i}[r_{ij}(C_{i,j-1}^{W} - C_{ij}^{W}) + r_{i,j+1}(C_{i,j+1}^{W} - C_{ij}^{W})],$$

$$j = 2, 3, \ldots, n_u - 1 \tag{25}$$

$$\left[\frac{\partial C_{i,nu}^{W}}{\partial t}\right]_{disp} = \frac{2\pi D_s \Delta s}{\nu \Delta V_{i,nu} \Delta u_i} r_{i,nu}(C_{i,nu-1}^{W} - C_{i,nu}^{W}) \tag{26}$$

$$\left[\frac{\partial C_{ij}^{W}}{\partial t}\right]_{disp} = \frac{2\pi D_s \Delta s}{\nu \Delta V_{i1} \Delta u_i}[2r_{i1}(C_i^{g}/K_H - C_{i1}^{W}) + r_{i2}(C_{i2}^{W} - C_{i1}^{W})] \tag{27}$$

Mass balances for dispersion transport of dissolved oxygen lead to similar expressions:

$$\left[\frac{\partial O_{ij}^{W}}{\partial t}\right]_{disp} = \frac{2\pi D_s \Delta s}{\nu \Delta V_{ij} \Delta u_i}\left[r_{ij}(O_{ij-1}^{W} - O_{ij}^{W}) + r_{ij+1}(O_{ij+1}^{W} - O_{ij}^{W})\right],$$

$$j = 2, 3, \ldots, n_u - 1 \quad (28)$$

$$\left[\frac{\partial O_{i,nu}^{W}}{\partial t}\right]_{disp} = \frac{2\pi D_s \Delta s}{\nu \Delta V_{i,nu} \Delta u_i} r_{i,nu}(O_{i,nu-1}^{W} - O_{i,nu}^{W}) \quad (29)$$

$$\left[\frac{\partial O_{ij}^{W}}{\partial t}\right]_{disp} = \frac{2\pi D_s \Delta s}{\nu \Delta V_{i1} \Delta u_i}\left[2r_{i1}(O_i^{g}/K_O - O_{i1}^{W}) + r_{i2}(O_{i2}^{W} - O_{i1}^{W})\right] \quad (30)$$

## Solution of NAPL Droplets

The solution of NAPL droplets is handled by assuming that the process is controlled by the rate of diffusion of dissolved VOC away from a droplet through a quiescent boundary layer, and that this diffusion process can be approximated as being in a steady state. The analysis is described in detail elsewhere (14), and leads to Eq. (31):

$$\frac{dC_{ij}^{N}}{dt} = -\frac{3C_0^{N} D_f}{\rho_{VOC} a_d^2}(C_{sat} - C_{ij}^{W})(C_{ij}^{N}/C_0^{N})^{1/3} \quad (31)$$

It is assumed here that the thickness of the quiescent boundary layer is large in comparison to the droplet radius.

## Gaseous Transport of VOC and Oxygen

It was shown earlier (see Eq. 18) that the volumetric air flow through any channel is given by $q = 1/K$ m$^3$/s. Carrying out a mass balance on gaseous VOC in the air channel segment in $\Delta V_i$ then yields

$$\nu\pi a_c^2 \Delta s \frac{dC_i^{g}}{dt} = q[C_{i+1}^{g}(P_i/P_{i+1}) - C_i^{g}] - \frac{4\pi D_s \Delta s a_c}{\Delta u_i}(C_i^{g}/K_H - C_{i1}^{W}) \quad (32)$$

where the first term on the right-hand side corresponds to advective transport in the gas phase and the second corresponds to dispersion transport of VOC into the air channel from the surrounding aqueous phase. The quotient of pressures in the first term corrects for the decrease in vapor-phase VOC concentration with decreasing pressure as the gas rises from the injection well. Note that as the pressure decreases the volumetric flux of the gas must increase correspondingly, resulting in an increased air

channel density as well. A virtually identical equation is obtained for gaseous oxygen:

$$v\pi a_c^2 \Delta s \frac{dO_i^g}{dt} = q[O_{i+1}^g(P_i/P_{i+1}) - O_i^g] - \frac{4\pi D_s \Delta s a_c}{\Delta u_i}(O_i^g/K_O - O_{i1}^W) \tag{33}$$

To avoid a system of equations which is mathematically stiff, we make the steady-state approximation for Eqs. (32) and (33), setting the derivatives on the left-hand sides equal to zero and solving for $C_i^g$ and $O_i^g$. This yields

$$C_i^g = \frac{AC_{i+1}^g + BC_{i1}^W}{C + D} \tag{34}$$

and

$$O_i^g = \frac{AO_{i+1}^g + BO_{i1}^W}{C + D'} \tag{35}$$

where

$$A = \frac{q(P_i/P_{i+1})}{v\pi a_c^2 \Delta s} \tag{36}$$

$$B = \frac{4D_s}{va_c \Delta u_i} \tag{37}$$

$$C = \frac{q}{v\pi a_c^2 \Delta s} \tag{38}$$

$$D = \frac{4D_s}{va_c \Delta u_i K_H} \tag{39}$$

$$D' = \frac{4D_s}{va_c \Delta u_i K_O} \tag{40}$$

The Henry's constant for oxygen, needed in Eqs. (28) and (40), is calculated by means of a least squares fit cubic expression in the temperature (here only, $T$ = °C),

$$K_O(T) \text{ (dimensionless)} = C_0 + T(C_1 + T(C_2 + TC_3)) \tag{41}$$

where $C_0 = 21.1043$, $C_1 = 0.5195226$, $C_2 = 2.171502 \times 10^{-3}$, $C_3 = -1.06668 \times 10^{-4}$, and the coefficient of determination over the temperature range 0–30°C is 0.9999965. Data for the fit were taken from Thibodeaux's book (19).

## The Model

The model consists of sets of differential equations for the $B_{ij}$, $C_{ij}^{N}$, $C_{ij}^{W}$, and $O_{ij}^{W}$, together with Eqs. (34) and (35) for the $C_i^g$ and $O_i^g$. The $B_{ij}$ and $C_{ij}^{N}$ are obtained from Eqs. (20) and (31). The $C_{ij}^{W}$ and $O_{ij}^{W}$ are obtained from

$$\frac{dC_{ij}^{W}}{dt} = \left[\frac{\partial C_{ij}^{W}}{\partial t}\right]_{bio} + \left[\frac{\partial C_{ij}^{W}}{\partial t}\right]_{disp} + \left[\frac{\partial C_{ij}^{W}}{\partial t}\right]_{soln} \tag{42}$$

and

$$\frac{dO_{ij}^{W}}{dt} = \left[\frac{\partial O_{ij}^{W}}{\partial t}\right]_{bio} + \left[\frac{\partial O_{ij}^{W}}{\partial t}\right]_{disp} \tag{43}$$

As the numerical integration proceeds, Eqs. (34) and (35) can be solved recursively since the values of $C_{ns+1}^{g}$ and $O_{ns+1}^{g}$ are known. The value of $C_{ns+1}^{g}$ is 0, assuming that the influent sparging air is uncontaminated. The value of $O_{ns+1}^{g}$ is given by $P(0)/P(h)$ times the ambient atmospheric concentration of oxygen (0.21 atm × 0.032 kg/mol)/(8.206 × $10^{-5}$ $m^3$·atm/mol·deg × $T$ °K).

The total residual mass of VOC remaining at time $t$ is obtained from

$$M_{tot}(t) = \sum_{i=1}^{n_s} \sum_{j=1}^{n_u} \Delta V_{ij}(\nu C_{ij}^{W} + C_{ij}^{N}) \tag{44}$$

## RESULTS

The model was implemented in TurboBASIC and run on Dell Dimension XPS computers with Pentium microprocessors operating at 75 and 133 MHz. Default values of the parameters used in the runs are given in Table 1. A typical run took approximately an hour on the faster machine.

The effect of the size of $K_{bio}$, the maximum rate of substrate degradation, is seen in Fig. 4. The values of $K_{bio}$ in these runs are 0, 0.1, 0.25, 1.0, 5, and 20 mg/kg/day, from top to bottom. Evidently the removal rate is not very sensitive to the value of $K_{bio}$, provided that it is 1 mg/kg/day or greater. Under these conditions the transport of oxygen from the air channels is the limiting factor. If $K_{bio} = 0$, so that there is no biodegradation, very pronounced tailing occurs as VOC at low concentrations must diffuse to the air channel. If biodegradation is occurring, on the other hand, diffusion limitation is due to the rate of transport of oxygen, which is diffusing from a high concentration in the air channel throughout the duration of the run. This reduces or eliminates the tailing observed in the absence of biodegradation.

TABLE 1
Default Parameter Values Used in the Modeling Runs

| | |
|---|---|
| Depth of horizontal pipe | 10 m |
| Half-width of air distribution at top of aquifer | 10 m |
| Length of horizontal pipe | 50 m |
| $q_z(x, z) = A(z)\cdot[(z/h)^m - (x/a)^n]$: $m$, $n$ | 1, 3 |
| Average air injection rate | 0.283 $m^3$/min (10 SCFM) |
| Air channel density parameter $K$ | $1 \times 10^6$ s/$m^3$ |
| Air channel mean diameter $2a_c$ | 1.0 cm |
| Aquifer porosity | 0.4 |
| Density of wet porous medium | 1.84 g/$cm^3$ |
| Dispersivity | $5 \times 10^{-8}$ $m^2$/s |
| Temperature | 15°C |
| $x$-Coordinate of top of tube of influence of channel | 9 m |
| Identity of VOC | Toluene |
| VOC solubility | 515 mg/L |
| Henry's constant of VOC (dimensionless) | 0.2081 |
| Density of VOC | 0.8716 g/$cm^3$ |
| Diffusivity of VOC in boundary layer | $2 \times 10^{-10}$ $m^2$/s |
| NAPL concentration | 0 mg/kg of soil |
| NAPL droplet diameter | 0.1 cm |
| Initial dissolved VOC concentration | 20 mg/L |
| Monod $K_{bio}$ | 0, 20 mg/kg/day |
| Biomass die-off constant $k_{die}$ | $2.5 \times 10^{-2}$ $day^{-1}$ |
| Biomass Monod parameter $B_{1/2}$ | 5 mg/kg of soil |
| VOC Monod parameter $C^W_{1/2}$ | 5 mg/L of water |
| Oxygen Monod parameter $O^W_{1/2}$ | 1 mg/L of water |
| VOC toxic inhibitory term $C^W_{tox}$ | 2000 mg/L of water |
| VOC toxic inhibitory exponent $n_{tox}$ | 3 |
| Weight biomass formed/weight substrate consumed | 0.5 |
| Weight oxygen consumed/weight substrate consumed | 3.126 |
| Initial biomass concentration | 5 mg/kg of soil |
| $\Delta t$ | 500 s |
| Duration of run | 500 days |



Comparison of Figs. 4, 5, 6, and 7 shows the effect of the air injection rate on the rates of cleanup by biosparging (bottom curves) and simple stripping (top curves). The air injection rates are 10, 25, 50, and 100 SCFM, respectively (1 SCFM = $4.719 \times 10^{-4}$ $m^3$/s). In these plots the values of $K$, the air channel density parameter, were adjusted to give the same air channel densities in all the runs. These values are $K$ = 10.0, 4.0, 2.0, and $1.0 \times 10^5$ s/$m^3$, respectively.

Comparison of Figs. 4, 8, and 9 shows the variation in cleanup rate as one moves from an air channel out near the periphery of the domain of

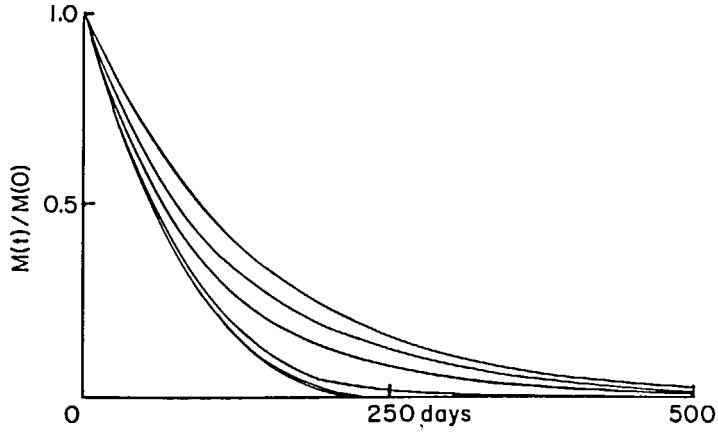


FIG. 4 Plots of reduced contaminant mass $M(t)/M(0)$ versus $t$; effect of $K_{bio}$. $K_{bio}$ = 0, 0.1, 0.25, 1.0, 5, and 20 mg/kg·day from the top down. Other parameters as in Table 1.



influence of the well ($x$-coordinate at the top of the channel = 9 m—Fig. 4) to more centrally located air channels. In Fig. 8 the $x$-coordinate at the top of the channel is 8 m; in Fig. 9 it is 7 m. The top and bottom curves of Fig. 4 should be used in these comparisons. In all cases, $K_{bio}$ is equal to 0 for the top curve and has a value of 20 mg/kg/day for the bottom

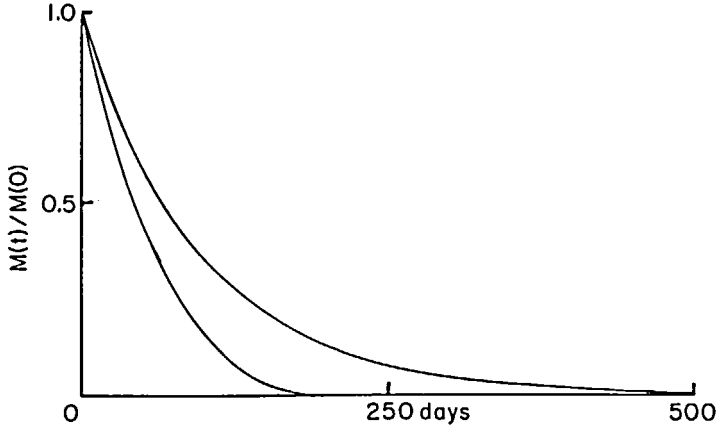


FIG. 5 Plots of reduced contaminant mass versus $t$; $K_{bio}$ = 0 and 20 mg/kg·day from the top down; air flow rate = 25 SCFM, $K = 4 \times 10^5$ s/m$^3$; other parameters as in Table 1.

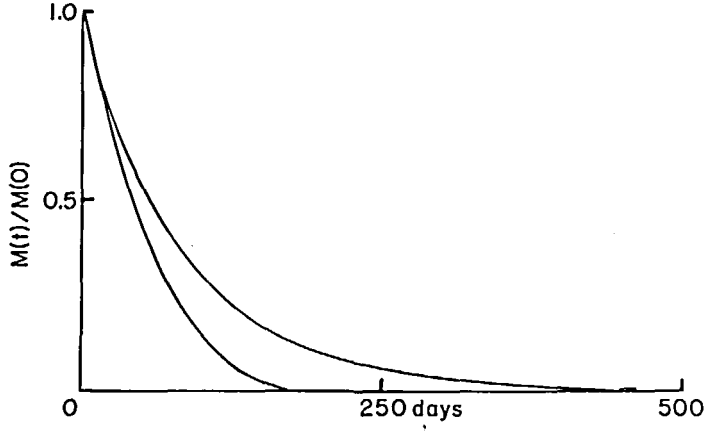


FIG. 6 Plots of reduced contaminant mass versus $t$; $K_{bio}$ = 0 and 20 mg/kg·day from the top down; air flow rate = 50 SCFM, $K = 2 \times 10^5$ s/m$^3$; other parameters as in Table 1.



curve. Out near the periphery of the domain the air flux is substantially reduced, so the channels are relatively far apart and remediation is slower than it is in tubes of influence which are more centrally located. Evidently one should space both sparging and biosparging wells sufficiently closely that there is substantial overlap between them in order to avoid having

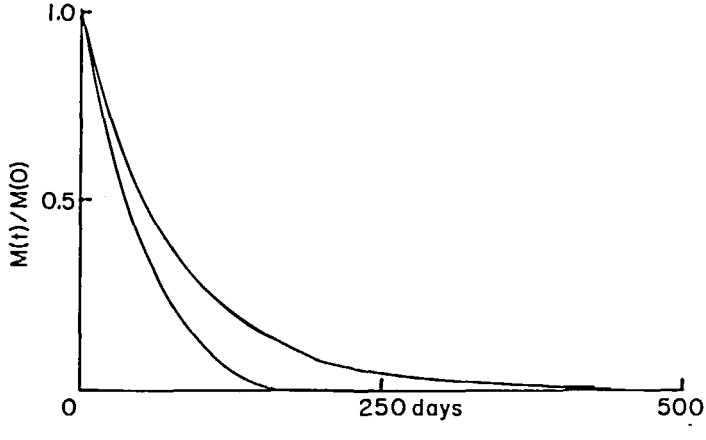


FIG. 7 Plots of reduced contaminant mass versus $t$; $K_{bio}$ = 0 and 20 mg/kg·day from the top down; air flow rate = 100 SCFM, $K = 1 \times 10^5$ s/m$^3$; other parameters as in Table 1.

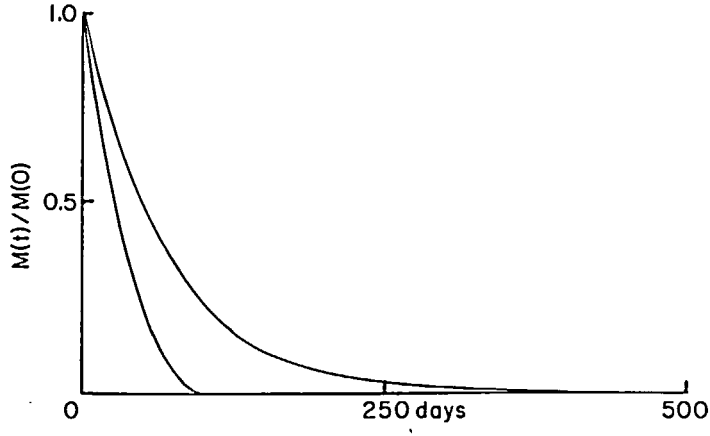


FIG. 8 Plots of reduced contaminant mass versus $t$; $K_{bio}$ = 0 and 20 mg/kg·day from the top down; $x$-coordinate at top of tube of influence of channel = 8 m; other parameters as in Table 1.



domains which are remediated too slowly. Closer spacing (overlap) also reduces the size of the area low in the domain between adjacent wells which receives no air. With both horizontal and vertical wells one expects that the width of the domain aerated increases as one moves up through the aquifer toward the water table. Using the width of the domain of

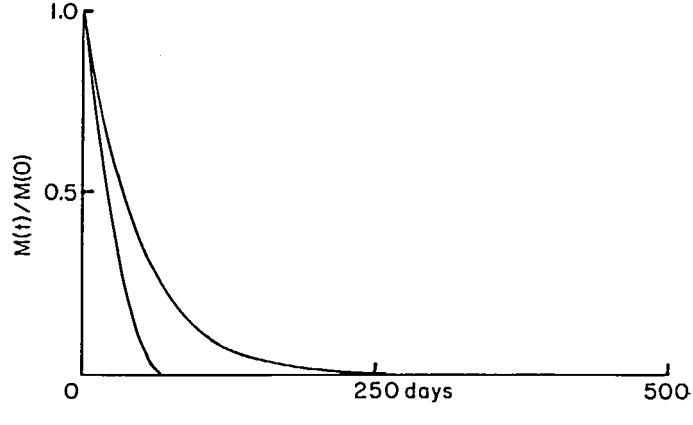


FIG. 9 Plots of reduced contaminant mass versus $t$; $K_{bio}$ = 0 and 20 mg/kg·day from the top down; $x$-coordinate at top of tube of influence of channel = 7 m; other parameters as in Table 1.

influence at the top of the aquifer as a basis for spacing the wells is likely to leave extensive regions in the lower portions of the contaminated zone which are not aerated and therefore not cleaned up.

Comparison of Fig. 6 with Fig. 10 shows the effect of the air channel density parameter $K$, which is $10^6$ s/m$^3$ for the runs in Fig. 6 and $10^5$ s/m$^3$ for those in Fig. 10. In both sets of runs the initial dissolved VOC concentration is 20 mg/L. As expected, cleanup rates are drastically reduced as $K$ decreases. The air channel density is proportional to $K$, so the spacings between channels (and the radii of the tubes of influence) increase with decreasing $K$, producing this result. One would expect aquifers with highly heterogeneous permeabilities to have relatively small values of $K$.

Comparison of Fig. 4 with Fig. 11 shows the effect of the diffusivity. In Fig. 4 the diffusivity is $5 \times 10^{-8}$ m$^2$/s; in Fig. 11 it is $2.5 \times 10^{-8}$ m$^2$/s. A twofold increase in the diffusivity is seen to result in very substantial increases in the rates of both biosparging and simple sparging without biodegradation. A number of workers have noted that one can increase the effective diffusivity by pulsed air injection, which produces local transient velocities in the groundwater in the vicinity of the sparging well.

Figures 4 and 12 show the effect of increasing the initial dissolved toluene concentration; in Fig. 4 this is 20 mg/L, while in Fig. 12 it is 100 mg/L. The top and bottom curves of Fig. 4 should be used for the comparisons. As expected, on a reduced mass basis there is no effect of initial concentra-



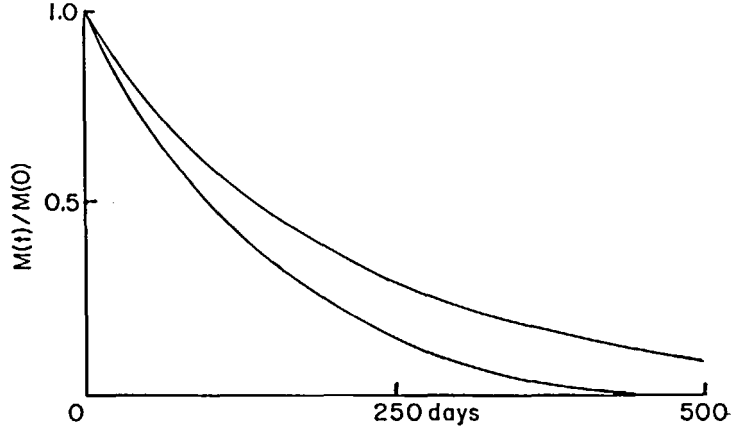


FIG. 10 Plots of reduced contaminant mass versus $t$; $K_{bio}$ = 0 and 20 mg/kg·day from the top down; air flow rate = 50 SCFM; $K = 1 \times 10^5$ s/m$^3$; other parameters as in Table 1.

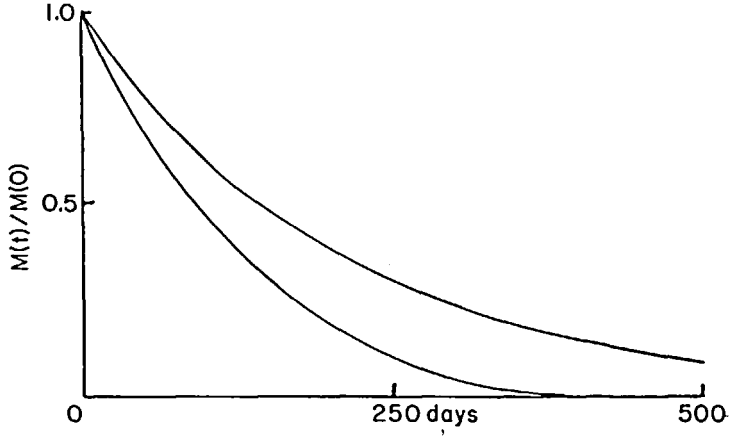


FIG. 11 Plots of reduced contaminant mass versus $t$; $K_{bio}$ = 0 and 20 mg/kg·day from the top down; dispersivity = $2.5 \times 10^{-8}$ m²/s; other parameters as in Table 1.



tion on the rate of removal by simple sparging. (The equations for this case are all linear.) For biosparging, the rate of reduced mass reduction is seen to decrease somewhat with increasing initial concentration. Since biodegradation goes from a first-order limit at very low VOC concentration to a zero-order limit at very high VOC concentrations, this result is expected.

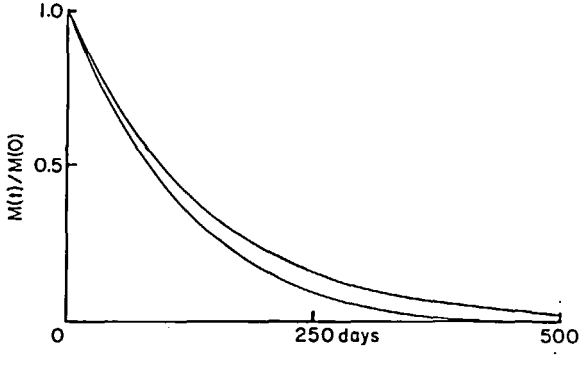


FIG. 12 Plots of reduced contaminant mass versus $t$; $K_{bio}$ = 0 and 20 mg/kg·day from the top down; initial dissolved contaminant concentration = 100 mg/L; other parameters as in Table 1.

Figures 4 and 13 compare the sparging and biosparging of toluene (Fig. 4) and *n*-octane (Fig. 13). The initial dissolved toluene concentration is 20 mg/L; the initial dissolved *n*-octane concentration is 0.67 mg/L (the assumed solubility), with a NAPL concentration of 19.33 mg/kg. As noted earlier (14, 17), the removal, by either simple sparging or biosparging, of a NAPL of quite low water solubility is an agonizingly slow process. The very low water solubility of *n*-octane implies that VOC concentration gradients will of necessity be quite small, so that mass transport of VOC to the air channels by dispersion will be quite small. Also, the very low maximum VOC concentrations which can be present mean that biodegradation rates will be quite small as well.

Figure 14 plots the radius of a tube of influence about an air channel which terminates at the water table at an $x$-coordinate of 9 m—i.e., the upper end of the air channel is at $(x, z) = (9, 10)$. In this figure $s$ is the arc length along the air channel measured from its upper end. We see the expected decrease in radius toward zero as the air injection point [at (0, 0)] is approached. The slight increase in the radius of the tube of influence as one moves down from the water table is perhaps unexpected. It is due to the fact that as one moves deeper below the surface of the aquifer, the hydrostatic pressure increases. This compresses the gas, resulting in a decrease in the volumetric gas flux. Since the air channel density is assumed proportional to the volumetric gas flux, this results in a decrease



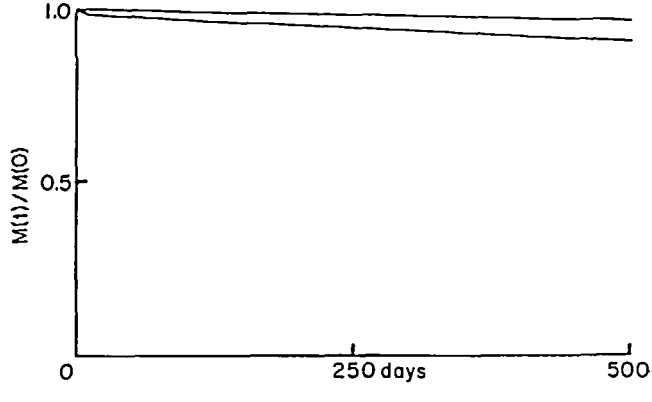


FIG. 13 Plots of reduced contaminant mass (*n*-octane) versus $t$; $K_{bio}$ = 0 and 20 mg/kg·day from the top down; initial dissolved *n*-octane concentration = 0.67 mg/L; VOC solubility = 0.67 mg/L; VOC Henry's constant = 131 (dimensionless); VOC density = 0.7925 g/mL; initial NAPL concentration = 19.33 mg/kg; mass of $O_2$ consumed per unit mass of VOC consumed = 3.502; other parameters as in Table 1.

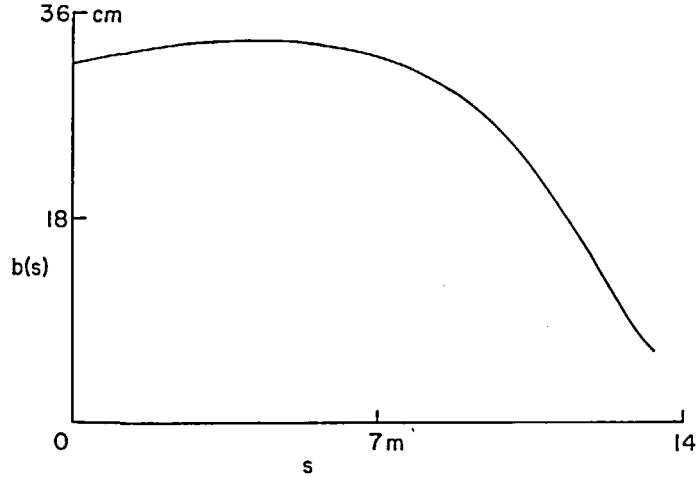


FIG. 14 Plot of radius of tube of influence about an air channel terminating at (9 m, 10 m). Parameters as in Table 1.



in air channel density and a corresponding modest increase in the radius of the tube of influence.

The air flow per channel in this model was shown earlier to be $q_{\text{channel}} = 1/K$. The default value of $K$, $1 \times 10^6$ s/m$^3$, gives a flow rate per channel of 60 mL/min. This, together with the default air flow rate, 10 SCFM, gives a total of 4720 air channels. The domain being stripped is 50 × 20 m, so there is an average of 4.72 channels/m$^2$, although the distribution is more dense near the axis of the domain and less dense out at the sides.

The radius of the tube of influence plotted in Fig. 14 varies from about 6 cm up to a maximum of about 33 cm at its upper terminus. The spacing of channel termini fairly near the edge of the domain is therefore about 66 cm, or a little over 2 feet. This does not appear to be seriously out of line with the field results obtained by Leeson et al. (21).

## CONCLUSIONS

The following conclusions can be drawn from this modeling work.

- Biosparging is effective at much lower average air flow rates than is sparging, provided that high enough instantaneous air flow rates are maintained during pulsed operation to give an adequate radius of influence of the well (or range of influence, for a horizontal well).

- Efforts to increase the dispersivity (generally by pulsed air injection) are well worth the trouble, since these can result in greatly increased biodegradation and stripping rates.
- Sparging wells should be placed substantially more closely together than one might expect on the basis of radius/range of influence measurements based on helium or $SF_6$ tracer distribution or mounding at the water table. Otherwise one is likely to have low-lying regions of contamination which are not aerated and therefore not remediated.
- Both the sparging and the biosparging of NAPL VOCs of quite low water solubility (such as alkanes) can be expected to be quite slow in comparison to the biodegradation and stripping of NAPL BTEX compounds, for instance.
- Remediation of aquifers having highly heterogeneous permeabilities (which contain silt/clay lenses or stringers, for example) will be very slow, because it will be difficult to impossible to deliver air to these structures.



## REFERENCES


1. R. E. Hinchee (Ed.), *Air Sparging for Site Remediation*, Battelle Press, Columbus, OH, 1993.
2. R. E. Hinchee, R. N. Miller, and P. C. Johnson, *In Situ Aeration: Air Sparging, Bioventing, and Related Remediation Processes*, Battelle Press, Columbus, OH, 1995.
3. W. C. Anderson (Ed.), *Innovative Site Remediation Technology: Bioremediation*, American Academy of Environmental Engineers, Annapolis, MD, 1995.
4. W. C. Anderson (Ed.), *Innovative Site Remediation Technology: Vacuum Vapor Extraction*, American Academy of Environmental Engineers, Annapolis, MD, 1995.
5. R. A. Brown, "Sparging: A New Technology for the Remediation of Aquifers Contaminated with Volatile Organic Compounds," in *Modeling of In Situ Techniques for Treatment of Contaminated Soils: Soil Vapor Extraction, Sparging, and Bioventing* (D. J. Wilson, Ed.), Technomic Publishing Co., Lancaster, PA, 1995.
6. M. E. Loden, *A Technology Assessment of Soil Vapor Extraction and Air Sparging*, US EPA Report EPA/600/R-92/273, Risk Reduction Engineering Laboratory, Office of Research and Development, US EPA, Cincinnati, OH, 1992.
7. B. A. Leeson, R. E. Hinchee, and C. M. Vogel, *Evaluation of the Effectiveness of Air Sparging*, Presented at In Situ and On-Site Bioreclamation: The Third International Symposium, April 24–27, 1995, San Diego, CA.
8. M. A. Dahmani, D. P. Ahlfeld, G. E. Hoag, and W. Ji, *Field Behavior of Air Sparging: Implications of a Conceptual Model*, Presented at In Situ and On-Site Bioreclamation: The Third International Symposium, April 24–27, 1995, San Diego, CA.
9. D. H. Mohr, *Mass Transfer Concepts Applied to In Situ Air Sparging*, Presented at In Situ and On-Site Bioreclamation: The Third International Symposium, April 24–27, 1995, San Diego, CA.
10. R. L. Johnson, N. R. Thomson, and P. C. Johnson, *Does Sustained Groundwater Circulation Occur during In Situ Air Sparging*, Presented at In Situ and On-Site Bioreclamation: The Third International Symposium, April 24–27, 1995, San Diego, CA.

11. F. C. Payne, A. R. Blaske, G. A vanHouten, and J. B. Lisiecki, *Comparison of Contan ination Removal Rates in Pulsed and Steady-Flow Aquifer Sparging*, Presented at I Situ and On-Site Bioreclamation: The Third International Symposium, April 24–2 1995, San Diego, CA.
12. D. H. Bass and R. A. Brown, *Performance of Air Sparging Systems—A Review Case Studies*, Paper 96-RP121B.01, Air & Waste Management Association 89th Annu Meeting and Exhibition, Nashville, TN, June 23–28, 1996, Abstracts, p. 200.
13. D. J. Wilson, C. Gomez-Lahoz, and J. M. Rodriguez-Maroto, "Groundwater Cleanu by In-Situ Sparging. VIII. Effect of Air Channeling on Dissolved Volatile Organ Compounds Removal Efficiency," *Sep. Sci. Technol.*, *29*, 2387 (1994).
14. D. J. Wilson, R. D. Norris, and A. N. Clarke, "Groundwater Cleanup by In-Si Sparging. IX. Air Channeling Model for Nonaqueous Phase Liguid Removal," *Ibid* *31*, 915 (1996).
15. D. J. Wilson, A. N. Clarke, K. M. Kaminski, and E. Y. Chang, "Groundwater Cleanu by In-Situ Sparging. XIII. Random Air Channels for Sparging of Dissolved and No aqueous Phase Volatiles," *Ibid.*, *32*(18), 2969 (1997).
16. W. Clayton, "Mass Transfer Modeling of In Situ Sparging Performance," in *Extende Abstracts, Industrial and Engineering Chemistry Special Symposium Emerging Tec nologies in Hazardous Waste Management VIII*, American Chemical Society, Birmin ham, AL, September 9–11, 1996, p. 791.
17. D. J. Wilson, R. D. Norris, and A. N. Clarke, "Groundwater Cleanup by In-Si Sparging. X. Air Channeling Model for Biosparging of Nonaqueous Phase Liquid, *Sep. Sci. Technol.*, *31*, 1357 (1996).
18. D. S. Kaback, B. B. Looney, J. C. Corey, L. M. Write, and J. L. Steele, "Horizont Wells for In Situ Remediation of Groundwater and Soils," in *Proceedings, NWW 3rd Outdoor Action Conference*, Orlando, FL.
19. L. J. Thibodeaux, *Environmental Chemodynamics*, 2nd ed., Wiley-Interscience, Ne York, NY, 1996.
20. D. J. Wilson, R. D. Norris, and R. D. Mutch Jr., "Groundwater Cleanup by In-Si Air Sparging. XI. An Improved Aeration Curtain Design," *Sep. Sci. Technol.*, *32*(16 2569 (1997).
21. A. Leeson, R. E. Hinchee, G. L. Headington, and C. M. Vogel, "Air Channel Distrib tion During Air Sparging. A Field Experiment", in *In Situ Aeration: Air Spargin Bioventing, and Related Remediation Processes* (R. E. Hinchee, R. N. Miller, and C. Johnson, Eds.), Battelle Press, Columbus, OH, 1995.

*Received by editor January 7, 1997*
*Revision received April 1997*